ACS OMEGA

Open Access

http://pubs.acs.org/journal/acsodf

Review

On the Use of the Intrinsic DNA Fluorescence for Monitoring Its Damage: A Contribution from Fundamental Studies

Dimitra Markovitsi*

Cite This: *ACS Omega* 2024, 9, 26826−26837

Read Online

ACCESS | Metrics & More | Article Recommendations

ABSTRACT: The assessment of DNA damage by means of appropriate fluorescent probes is widely spread. In the specific case of UV-induced damage, it has been suggested to use the emission of dimeric photoproducts as an internal indicator for the efficacy of spermicidal lamps. However, in the light of fundamental studies on the UV-induced processes, outlined in this review, this is not straightforward. It is by now well established that, in addition to photodimers formed via an electronic excited state, photoionization also takes place with comparable or higher quantum yields, depending on the irradiation wavelength. Among the multitude of final lesions, some have been fully characterized, but others remain unknown; some of them may emit, while others go undetected upon monitoring fluorescence, the result being strongly dependent on both the irradiation and the excitation wavelength. In contrast, the fluorescence of undamaged nucleobases associated with emission from $\pi\pi^*$ states, localized or excitonic, appearing at wavelengths shorter than 330 nm is worthy of being explored to this end. Despite its low quantum yield, it is readily detected nowadays. Its intensity decreases due to the disappearance of the reacting nucleobases and the loss of exciton coherence provoked by the presence of lesions, independently of their type. Thus, it could potentially provide valuable information about the DNA damage induced, not only by UV radiation but also by other sanitizing or therapeutic agents.

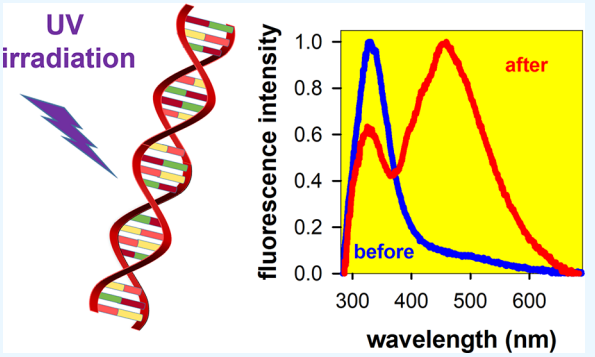

1. INTRODUCTION

Numerous studies report detection of DNA damage by monitoring the fluorescence of appropriate labels chemically attached to nucleic acids, of intercalating dyes, or even that of tryptophane and tyrosine present in bacterial membranes,[1−11] with the objective to control the progress of therapeutic treatments or the efficacy of various sanitizing agents. In the specific case of damage induced by UV radiation, an alternative method was suggested, exploiting the emission of a particular class of UV-induced lesions, the pyrimidine (6−4) pyrimidone photoadducts (abbreviated as 64PP). It was first proposed five decades ago by Hauswirth and Wang, who examined a series of model dimeric compounds, as well as calf thymus and influenza virus DNA in solution.[12] They found that the fluorescence intensity monitored at 400 nm with excitation at 310 nm increases linearly with the irradiation dose. This perspective resurfaced recently, in the context of the COVID-19 pandemic, with the increasing utilization of germicidal lamps for disinfection purposes.[13−19] Surprisingly, despite the fact that the SARS-CoV-2 virus genome is composed of single-stranded ARN, the most recent studies focused mainly on thymine phototoproducts.[20,21] The fingerprint of 64PP was searched in irradiated DNA duplexes, both synthetic and genomic; while the authors concluded that their emission appears in the systems containing adenine-thymine pairs, they also noticed unexpected spectral alterations in the absence of such pairs.[21]

From an opposite standpoint, the alteration of the intrinsic DNA fluorescence during spectroscopic measurements has been a serious obstacle to its characterization (Figure 1). However, the problem was overcome thanks to specific experimental protocols.[22,23] Boosted by the development of the femtosecond spectroscopy[23−26] and the availability of UV-sensitive detectors, our understanding of the DNA fluorescence advanced rapidly. It was shown that its properties are modulated by the secondary structure, with the electronic coupling among nucleobases playing a pivotal role.[23,27] Recently, the use of the intrinsic fluorescence of nucleic acids for analytical purposes, such as the screening of a large number of sequences,[28] the detection of target DNA[29] and Pb^{2+} ions,[30] or the authentication of COVID-19 vaccines,[31] started to be explored.

Received: March 7, 2024
Revised: May 2, 2024
Accepted: May 8, 2024
Published: June 13, 2024

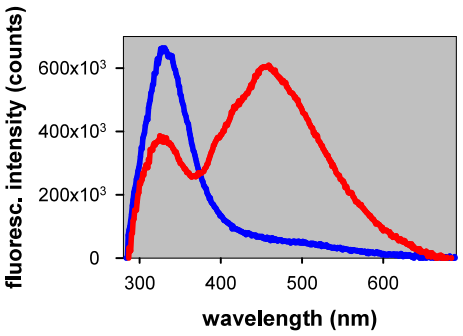

Figure 1. Alteration of the fluorescence of calf thymus DNA due to its damage by femtosecond laser pulses at 267 nm. Fluorescence spectra recorded exciting at 255 nm before (blue) and after (red) irradiation. Reprinted from ref 32. Copyright ACS 2010.

In parallel, our comprehension of the fundamental processes leading to DNA damage upon direct UV absorption made considerable progress. The picture emerging from time-resolved spectroscopic techniques, associated with computational and analytical methods, is more complex than initially thought. Thus, for example, it was shown that energy transfer among nucleobases provokes remote photodamage[33] and that photoinduced charge separation may lead to self-repair of the damage in the absence of proteins.[34] Likewise, it was evidenced that photoionization, more efficient at short wavelengths,[35] is still operative over the entire absorption spectrum of DNA.[36]

The objective of the present review is to examine how the changes, both chemical and conformational, resulting from the DNA damage, may affect its intrinsic fluorescence. It is not intended to be exhaustive regarding the various aspects that are tackled—such specialized reviews already exist and they are cited. It simply outlines recent advances on the fundamental processes triggered in DNA by direct photon absorption, whose outcomes have not yet penetrated the scientific communities working on the DNA damage, as well as on the development of UV sanitizing equipment and associated sensing devices. It endeavors to establish a connection among topics that are usually not treated together. The effort is worth it because, should the above approach prove reliable, it would greatly facilitate the development of sensing devices. The reason is that it does not require the synthesis of nucleic acids containing labels and bypasses uncertainties arising from noncovalent interactions between nucleic acids and dyes.

The review is structured as follows. In Section 2 we examine the main factors governing the fluorescence of undamaged DNA. In Section 3 we discuss the fluorescence properties of dimeric photoproducts in relation with the quantum yields of their formation. In Section 4 we present the photoionization mechanisms, comparing their efficiency with those of photodimerization reactions. In Section 5 we discuss in a global way the effect of the DNA damage on its intrinsic fluorescence. Finally, we argue that the decrease of the intrinsic fluorescence of undamaged DNA at short wavelengths should be more informative regarding its damage compared to that of the numerous lesions.

2. FLUORESCENCE OF UNDAMAGED DNA

Measurements on the intrinsic fluorescence of undamaged DNA reported in the recent literature concern, in addition to steady-state spectra, the determination of fluorescence decays and fluorescence anisotropies from the femtosecond to the nanosecond time scales, as well as time-resolved spectra.[23−25,37−42] The latter have largely contributed to comprehending the factors governing photon emission. The main outcomes of these studies are highlighted in ref 23. The emission stemming from guanine quadruplexes (G-quadruplexes) is outlined in ref 43, in view of its potential application in biosensors. Below we focus mainly on single and double strands, drawing attention to aspects that are important in relation to damage detection.

2.1. Large Range of Quantum Yields. The early observation that the fluorescence quantum yields (Φ_{fl}) of nucleic acids at room temperature are extremely low,[44] associated with the above-mentioned technical difficulties to characterize its emission properties correctly, created the reputation of DNA as nonfluorescent. However, the most recent studies showed that the Φ_{fl} of nucleic acids exhibits variations of at least 2 orders of magnitude, depending on the examined system and the excitation wavelength.

The Φ_{fl} determined for the mononucleosides and mononucleotides of the four major bases fall in the range of $(0.7-1.5) \times 10^{-4}$.[45] Such low values, concomitant to ultrafast decays of their bright excited states, are due to the existence of conical intersections connecting the potential energy surfaces of the first singlet excited state and the ground state.[46] However, the monomeric chromophores of minor, also naturally occurring nucleobases, such as the epigenetic ones, may exhibit significantly higher Φ_{fl} values; for example, 5.6×10^{-4} for 5-methyl cytidine[47] or 3.8×10^{-3} for N7-methyl guanosine.[48]

Going form monomeric to multimeric nucleic acids, the fluorescence behavior becomes much more complex, strongly depending on the secondary structure. The ranges of the Φ_{fl} values determined for monomers and multimers[23,43,49−51] containing solely major nucleobases are depicted as histograms in Figure 2. Notably, the emission of G-quadruplexes may be up to 1 order of magnitude more intense compared to their constitutive monomeric chromophores.[43]

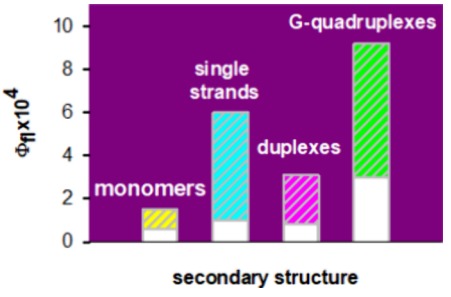

Figure 2. Dependence of the fluorescence quantum yield on the secondary DNA structure: mononucleotides (yellow), single strands (cyan), duplexes (pink), and G-quadruplexes (green). The shaded areas indicate the range of Φ_{fl} values determined for each type of structure with excitation at 255−270 nm.

When the excitation wavelength moves toward longer wavelengths, dramatic changes are observed in the fluorescence. In this respect, we note that both genomic and synthetic DNA exhibit a long absorption tail extending over the UVA spectral domain.[52,53] And the Φ_{fl} determined for the duplex dA_{20}•dT_{20} with excitation at 335 nm (2×10^{-2}) is 2 orders of magnitude higher than that determined for the same system with excitation at 267 (3×10^{-4}).[54] Moreover, the UVA induced fluorescence of dA_{20}•dT_{20} is significantly higher compared to that of its constitutive single stands dA_{20} and dT_{20} (Figure 3).

https://doi.org/10.1021/acsomega.4c02256
ACS Omega 2024, 9, 26826−26837

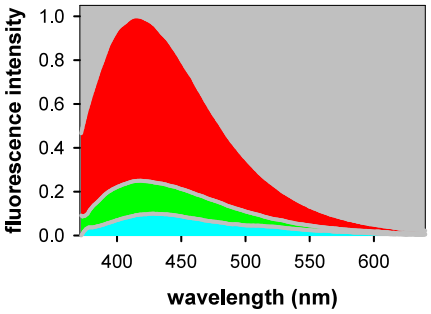

Figure 3. Steady-state fluorescence spectra of dA_{20}•dT_{20}, (red), dA_{20} (green), and dT_{20} (cyan). Excitation wavelength: 335 nm. The spectral areas are proportional to the quantum yields. Adapted from ref 54. Copyright ACS 2011.

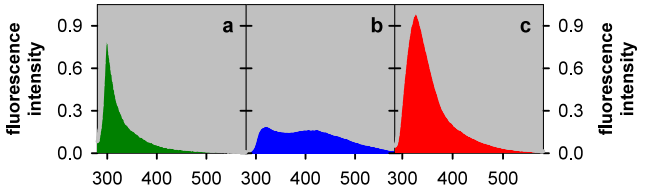

Figure 4. Steady-state fluorescence spectra of polymeric duplexes with simple repetitive sequence. The spectral areas are proportional to the quantum yields (a) $d(GC)_n$•$d(GC)_n$, $\Phi_{fl} = 1.5 \times 10^{-4}$; (b) $d(AT)_n$•$d(AT)_n$, $\Phi_{fl} = 1.4 \times 10^{-4}$; (c) dA_n•dT_n, $\Phi_{fl} = 3 \times 10^{-4}$. Excitation wavelength: 267 nm. Adapted from references 63 and 42. Copyright ACS 2010 and 2023.

2.2. Excited States Responsible for DNA Fluorescence. Due to the proximity of nucleobases within DNA multimers, they may be electronically coupled. This means that the excited states are delocalized over two or more of them (collective states). The electronic coupling depends on both the type of nucleobases and their geometrical arrangement. It determines the excited states responsible for photon absorption giving rise to the well-known hypochromism[55,56] exhibited by duplexes at 260 nm and the long absorption tail in the UVA spectral domain.[57] It also affects the shape of the fluorescence spectra and the associated quantum yields (Figure 3).

For a specific sequence and secondary structure, the electronic coupling is influenced by the conformational disorder of the nucleic acid.[58,59] The amplitude of this disorder depends on the duplex size[60,61] and the ionic strength of the solution,[62] both factors affecting the DNA photophysical properties.[23,42]

Given the dependence of the electronic coupling on the conformational disorder, the absorption and fluorescence spectra of DNA multimers are the envelope of a multitude of electronic transitions. Emission stems from various types of electronic excited states, localized on individual nucleobases or collective, some of them being stronger emitters than others. We can distinguish two limiting cases of collective emitting states: excitons, which can be viewed as linear combinations of the bright excited states ($\pi\pi^*$) of individual nucleobases; and excited charge transfer (*CT*) states, involving two stacked nucleobases, with an atomic charge being transferred between them. However, the majority of the emitting states have mixed $\pi\pi^*/CT$ character.

In duplexes, the fingerprint of collective states with dominant exciton character appears mainly at short wavelengths of their emission spectrum; they can be differentiated from the localized $\pi\pi^*$ states via their lifetime and their anisotropy.[23,42] A typical example is the duplex $d(GC)_n$•$d(GC)_n$, whose narrow fluorescence spectrum, peaking at ~300 nm (Figure 4a), has been correlated with excitons extended over at least four nucleobases across both strands.[64] *CT* states are devoid of oscillator strength and, in principle, do not fluoresce. But if the charge transfer is not complete, they may emit weakly at long wavelengths; their fluorescence usually appears as a long tail on the visible spectral domain. Finally, some nucleic acids exhibit a second emission band, located at longer wavelengths compared to the $\pi\pi^*$ emission and attributed to excimers/exciplexes. This is the case of polymeric duplexes $d(AT)_n$•$d(AT)_n$ duplexes,[24,65] whose fluorescence peaks at 320 and 407 nm in (Figure 4b).[66] For comparison, we mention that the fluorescence maxima of all mononucleosides and mononucleotides are located below 334 nm,[45] while those of equimolar mixtures corresponding to G•C and A•T pairs at 330 and 325 nm, respectively.[42]

2.3. Strand Flexibility: A Key Player. Once an excited state is populated by photon absorption within a DNA multimer, the system finds itself out of equilibrium and, before decaying to the ground state, it starts evolving so that to minimize its energy. This process involves small geometrical rearrangements of the nucleic acid itself, as well as reorganization of the aqueous solvent and the metal cations in the vicinity. The extent in which such modifications take effectively place depends on the flexibility of the system. Conformational motions have a dramatic effect on the excited state relaxation and, hence, on the fluorescence. First, they tend to break down the coherence of the exciton states formed by photon absorption. The latter may evolve toward either $\pi\pi^*$ states localized on single nucleobases or toward *CT* states. Depending on the degrees of freedom, it is also possible that the system reaches a minimum in the potential energy surface of the first excited state involving two nucleobases (excimers or exciplexes). Below we provide some examples illustrating how these effects are manifested in the emission spectra.

The rigidity of a duplex increases, among others, with the number of hydrogen bonds per base pair: two for A•T pairs, three for G•C pairs. Thus, the fluorescence spectrum of $d(GC)_n$•$d(GC)_n$, dominated by emission stemming from long-lived excited states with strong exciton character, is narrower and located at shorter wavelengths compared to those of $d(AT)_n$•$d(AT)_n$ and $d(A)_n$•$d(T)_n$ (Figures 4b and 4c). Although the spectra of the latter duplexes also contain such exciton components,[66,67] their contribution is smaller and other types of emitting states are dominant.

Following the same reasoning, a given DNA sequence is much more flexible as a single strand than when it is paired, forming a duplex. Consequently, excimer/exciplex formation is easier in single than in double strands. This is shown in Figure 5, where the fluorescence spectra of two duplexes are presented together with that of their purine-rich constitutive strand. The latter, although they have numerous degrees of freedom, are sufficiently structured so that to allow the interaction between nucleobases. For the system with a random base sequence (Figure 5a), we observe two peaks both for the single and the double strand, at 326/322 nm and at 436 nm. But their relative intensity is inversed, that at 436 nm being dominant in the case of the single strand. A more drastic change is encountered for adenine tracts. When they are paired with thymine single strands, the adenine excimer band, peaking at 360 nm, is completely suppressed and the entire fluorescence spectrum is shifted to shorter wavelengths, peaking at 327 nm (Figure 5b). This difference has been rationalized by quantum chemical

https://doi.org/10.1021/acsomega.4c02256
ACS Omega 2024, 9, 26826−26837

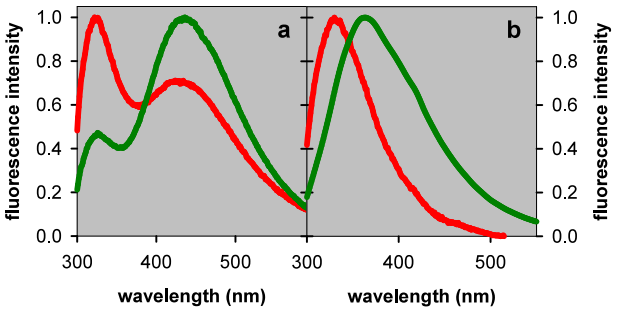

Figure 5. Comparison of duplex fluorescence spectra (red) with that of the constitutive purine rich single strand (green). (a) d(CGGACAAGAAG)•d(CTTCTTGTCCG) and d(CGGACAAGAAG). Adapted from ref 51. Copyright RSC 2013. (b) $d(A)_{20}$•$d(T)_{20}$ and $d(A)_{20}$. Adapted from ref 54. Copyright ACS 2007. Excitation wavelength: 267 nm. The intensities are normalized at the maximum.

calculations, which showed that structural constrains within the duplex prevent the two involved adenines to adopt the geometrical arrangement corresponding to the excimer.[50,68]

A comparison between the duplexes $d(AT)_n$•$d(AT)_n$ and $d(A)_n$•$d(T)_n$ is also instructive. Molecular dynamics simulations have shown that the amplitude of conformational motions is significantly higher in the former duplex.[58] Thus, configurations appropriate for adenine-thymine exciplexes are more likely to be reached in the case of the alternating sequence, explaining the appearance of a second peak in its fluorescence spectrum (Figure 4b).

In a more general way, any external factor hindering conformational motions enhances the DNA fluorescence.[69] The most striking effect is observed upon temperature lowering: the Φ_{fl} at 77 K is 2 orders of magnitude higher compared to room temperature;[44] that is why the early studies on DNA fluorescence were performed at such low temperatures.[70,71] An important enhancement is caused also by increasing the viscosity of the solution.[72]

3. PHOTODIMERS

In this Section we examine the DNA lesions resulting from reactions that occur on an excited state and involve two nucleobases. The main representatives are cyclobutane pyrimidine dimers (CPD) and 64PP;[73] those formed by two thymines are shown in Figure 6. But other types of photodimers are also known. Although thousands of publications deal with photodimers, only a few of them discuss fundamental processes related to their formation, describe their photophysical properties or report quantum yields. And below we focus mainly on them.

3.1. Cyclobutane Pyrimidine Dimers. CPD are the most abundant dimeric photoproducts formed following UV irradiation in both purified genomic DNA in solution (Table 1) and in cellular DNA.[73] They absorb below 260 nm[74] and

Table 1. Quantum yields ($\Phi \times 10^4$) Determined for the Formation of Selected Photoinduced Species in Genomic DNA Following Irradiation at 254/266 nm

CPD[a]	64PP[a]	AA*[b]	A=A[b]	TA*[a]	(G−H)•[a]	8-oxodG[a]
9.8[79]	3.2[79]	0.06[80]	0.19[80]	0.14[81]	20[36]	0.5[82]

[a]Calf thymus DNA. [b]*Escherichia coli*.

irradiation at their absorption band induces the reverse reaction, regenerating the initial pyrimidines with a quantum yield close to 1. There is no report on their fluorescence.

The excited states responsible for CPD formation are exciton states, whose population requires an appropriate geometrical arrangement.[27,75] Their population in a given pyrimidine-pyrimidine step is affected by neighboring nucleobases, with which they may form *CT* states.[76] Femtosecond transient absorption experiments on thymine single strands showed that the CPD formation occurs within 1 ps.[77] The quantum yield of their formation (Φ_{CPD}) in these strands is constant along the main absorption spectrum (50×10^{-3}), but it drops abruptly to 10^{-4} for UVA irradiation,[49] because exciton states are not populated directly by UVA.[78] While the Φ_{CPD} determined for UVC excitation decreases upon base pairing, the opposite trend is observed for UVA irradiation.[54]

Coming to duplexes, the Φ_{CPD} reported in the case of $d(A)_{20}$•$d(T)_{20}$ is 22×10^{-3} and 0.5×10^{-3} for excitation at 266 and 330 nm, respectively.[54] In double-stranded calf thymus DNA, the thymine CPD represent *ca.* 56% of the ensemble of detected CPD ($\Phi_{CPD} \sim 10^{-3}$, Table 1), this percentage being affected by the ionic strength of the solution and the temperature.[79]

3.2. Pyrimidine (6−4) Pyrimidone Photoadducts. According to quantum chemical calculations, 64PP are formed via an excited *CT* state.[27] In TC steps, the reaction evolves directly toward the 64PP, while in TT and CT steps, an oxetane intermediate is initially formed. Transient absorption measurements on $(dT)_{20}$ showed that the oxetane intermediate is transformed to 64PP within 4 ms.[83] Moreover, the existence of an energy barrier in the photoreaction leading to the oxetane intermediate accounts for the decrease of the quantum yield (Φ_{64}) for T-T 64PP observed upon increasing the irradiation

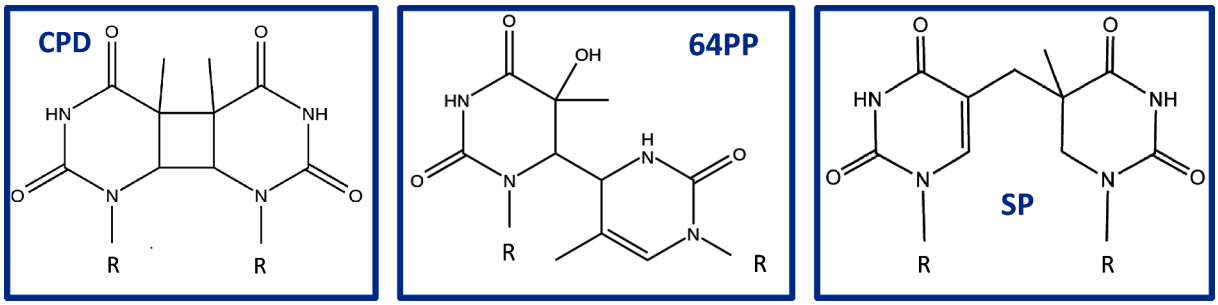

Figure 6. Chemical formulas of thymine dimers: cyclobutane dimer (CPD), (6−4) photoadduct (64PP), and spore photoproduct (SP). R denotes the backbone.

https://doi.org/10.1021/acsomega.4c02256
ACS Omega 2024, 9, 26826−26837

wavelength.[49] The direct, one-step mechanism, explains why the quantum yield of T-C 64PP in calf thymus DNA is significantly higher compared to those of the T-T and C-T analogs (Table 2); no C−C 64PP were detected in this case.[79]

Table 2. Selected Properties of Pyrimidine (6-4) Pyrimidone Photoadducts

	$\Phi_{64} \times 10^4$[a]	$\lambda_{abs,max}$[b] (nm)	ε_{max}[b] (L mol^{-1}cm^{-1})	$\lambda_{fl,max}$[b] (nm)	Φ_{fl}[b]
T-T	0.33	325	4600	393	0.028
T-C	2.86	315	1400	397	0.007
C-T	0.01	325	3500	400	0.015

[a]Formation quantum yields (Φ_{64}) in double-stranded calf thymus DNA for irradiation at 254 nm.[79] [b]Photophysical properties determined for dinucleoside monophosphates 64PP; $\lambda_{abs,max}$: absorption maximum; ε_{max}: maximum molar absorption coefficient; $\lambda_{fl,max}$: fluorescence maximum.[84,85]

Hauswirth and Wang determined the Φ_{fl} of model 64PP formed just by two pyrimidines.[12] Two decades later, Blais et al. published an extensive study on the 64PP fluorescence and evidenced the effect of various factors (types of nucleobases, phosphate group, dehydration) on both their absorption and emission spectra, as well as on their Φ_{fl} (Table 2).[84] That found for the T-T 64PP (0.028) is in good agreement with the value determined later by Marguet and Markovitsi for the same lesion formed within $(dT)_{20}$, whose fluorescence maximum is located at 394 ± 2 nm (Figure 7).[83]

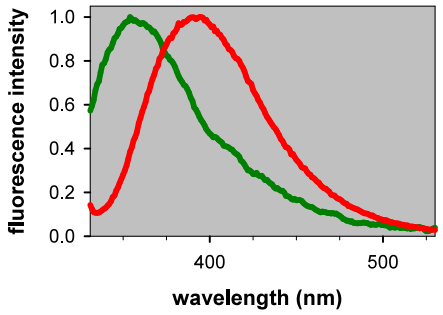

Figure 7. Normalized steady-state fluorescence spectra. Red: $(dT)_{20}$ after irradiation at 255 nm (excitation at 320 nm). Green: 8-oxodG (excitation at 255 nm). Adapted from references 49 and 86. Copyright ACS 2005 and 2012.

In view of the Φ_{64} and Φ_{fl} values in Table 2, it appears that for relatively short excitation wavelengths (290−315 nm) of irradiated double-stranded calf thymus DNA, T-C 64PP should be stronger emitters than that T-T 64PP. And their combined fluorescence is expected to peak a slightly below 400 nm.

Light absorption by 64PP leads to formation of Dewar valence isomers which are not fluorescent.[87] A study of T-T 64PP, combing time-resolved experiments and quantum chemistry calculations, showed that the formation of Dewar valence isomers takes place on the excited singlet state with a quantum yield of about 8%.[88]

3.3. Spore Photoproduct. Although this review is concerned with the processes taking place in purified DNA dissolved in aqueous solution, we cannot omit to mention the so-called spore photoproduct (SP),[89] which is formed in microbial organisms, targeted precisely by the sanitizing UV lamps. Its formation involves two thymines and was identified as 5-thyminyl-5,6-dihydrothymine (Figure 6). When the hydration of DNA is low and it adopts A-form configuration, SP is by far the dominant bispyrimidine photoproduct detected following UVC irradiation (93%). Its absorption spectrum peaks at 265 nm with a molar absorption coefficient of 8200 $M^{-1}Lcm^{-1}$. There is no information regarding its fluorescence properties.

3.4. Other Types of Photodimers. Early experiments demonstrated that irradiation at 254 nm leads to the formation of two different types of adenine dimers, AA* and A = A (Figure 8), and suggested that they have a common azetidine

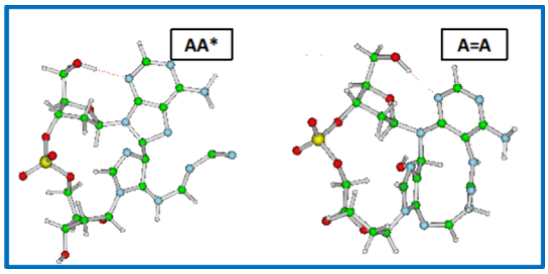

Figure 8. Schematic drawing of the two adenine photodimers. Reprinted from ref 91. Copyright ACS 2016.

intermediate.[90] Later, studies combining quantum chemistry, molecular dynamics and time-resolved spectroscopy, identified the reaction path in the first excited state leading to this intermediate, whose lifetime is comprised between 2 s and a few minutes.[91] The quantum yield for adenine dimer formation in $(dA)_n$ is 3×10^{-3}, but it drops by at least 1 order of magnitude in double-stranded DNA (Table 1).[80]

A dimeric photoproduct, coined TA* and identified as 1,3-diazacyclooctatriene, is formed only in TA steps with a quantum yield of 5×10^{-4} in $(dAT)_n$ single strands, 1×10^{-4} in $d(AT)_n \bullet d(AT)_n$ and 1.4×10^{-5} in duplex calf thymus DNA.[92,93] When generated in dTpdA dinucleotides, its absorption appears at longer wavelengths, between 290 and 340 nm.[81] The reaction involves a cyclobutane-like intermediate formed from an exciton state with significant *CT* character.[94] Another "adenine-thymine" reaction product was detected in irradiated calf thymus DNA;[95] although its quantum yield is at least twice as high as that of TA*, its structure has not been characterized yet.

According to an article published in 1986, adenine−adenine, adenine-thymine, adenine-guanine and guanine−guanine photodimers would give rise to more or less intense fluorescence.[96] However, those measurements were not performed with well-defined structures, as determined in later studies.

4. PHOTOIONIZATION

In this section we discuss the one-photon ionization process, according to which a single photon absorbed directly by DNA induces ejection of an electron and generates an electron hole (radical cation) on the nucleic acid. Radical cations are precursors to oxidative damage. The study of photoionization by nanosecond transient absorption has brought valuable information because it allows determination of the associated quantum yields Φ_i and characterizes the time evolution of the generated radicals in a quantitative way. Intense laser sources may provoke two-photon ionization, according to which a first photon populates an excited state, while a second photon absorbed by this excited state provokes electron ejection. This method allows discriminating chemical species formed in an

https://doi.org/10.1021/acsomega.4c02256
ACS Omega 2024, 9, 26826−26837

Table 3. Photoionization Quantum Yields at 266 nm ($\Phi_i \times 10^3$) of Selected Single and Double Strands[a]

$d(T)_{20}$	$d(A)_{20}$	$d(A)_{20}\bullet d(T)_{20}$	$d(AT)_{10}\bullet d(AT)_{10}$	$d(GC)_5\bullet d(GC)_5$	CT-DNA[b]
<0.5	1.1 ± 0.1	1.4 ± 0.1	1.1 ± 0.2	1.2 ± 0.2	2.0 ± 0.2

[a]Values from reference 36. Copyright ACS 2020. [b]Calf thymus DNA.

excited state from those stemming from radical cations, whose ratio decreases with increasing laser.[91,97−99]

4.1. Two Different Mechanisms of Electron Photoejection. For long it was considered that only high-energy photons, corresponding typically to wavelengths shorter than 210 nm, are capable of ionizing DNA. But on 2005, Kawai et al. observed electron ejection from a telomeric G-quadruplex following UVB irradiation.[100] Later on, more sensitive experiments, performed with 266 nm excitation, determined one-photon ionization quantum yields (Φ_i) for a large number of DNA structures. These measurements, combined to quantum chemistry calculations,[27] revealed that the low-energy photoionization mechanism differs from that operative at high-energies.[36,101]

At high energies, the electron is detached directly upon photon absorption, without any prior geometrical rearrangement. The Φ_i of calf thymus DNA at 193 nm (0.04[102]/0.06[103]) is roughly the average of the values found for its monomeric constituents.

At low-energies, Φ_i depends strongly on the secondary structure. The highest values, up to 1.5×10^{-2}, were found for G-Quadruplexes,[43] but could not be determined for mononucleosides and mononucleotides ($\Phi_i < 5 \times 10^{-4}$). Those obtained for selected single and double strands are presented in Table 3.

Low-energy photoionization takes place via a multistep indirect mechanism. A small fraction of the *CT* states populated during the excited state relaxation may undergo charge separation, already evidenced for DNA.[34,104] Finally, under the effect of conformational motions, which may prevent charge recombination, the electron is ejected from the "negatively charged" nucleobase, whose ionization potential is much lower compared to that of "neutral" ones. In view of this mechanism, electron ejection is in principle possible as far as photon absorption leads to the population of a *CT* state, explaining its observation upon UVB irradiation.[100]

The electron holes formed either via high- or via low-energy irradiation, following a charge transfer process, eventually reach the sites with the lowest oxidation potential, i.e. guanines, or, in the absence of guanines, adenines.[36,105,106] In all cases, the concentration of the generated purine radicals was found to be the same as that of the hydrated ejected electrons.

As the Φ_i values determined for high-energy photoionization are much higher than those found for the low-energy process (20−30 times for calf thymus DNA), far-UVC lamps are likely to be more efficient in provoking oxidative damage than the medium range UVC lamps. This contrasts with Φ_{CPD}, which is constant over the wavelengths corresponding to the thymine $\pi\pi^*$ transitions.[49] And the maximum molar absorption coefficients of the thymidine chromophore are similar at high and low-energies.[107]

4.2. Fate of Generated Radical Cations. Purine radical cations are unstable in neutral aqueous solution and tend to lose a proton. The proton lost by the guanine radical cation in single and double strands is shown in Figure 9a; a more complex pattern was found in G-quadruplexes, described in detail in references 108 and 109. The deprotonation process in single and double strands, occurring on the nanosecond time scale,[109,110] is

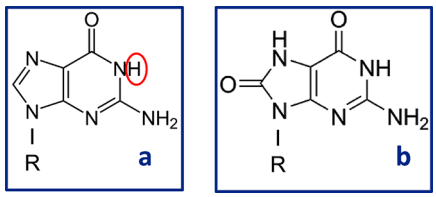

Figure 9. Chemical formulas of (a) guanosine and (b) 8-oxodG. The proton encircled in (a) is that lost upon deprotonation of the radical cation in single and double strands. R denotes the backbone.

faster than other reaction paths. Consequently, the quasi-entire population of the radical cations undergoes deprotonation. In calf thymus DNA, the quantum yield for the formation of deprotonated radicals $(G\text{-}H)^\bullet$ at 266 nm equals that of the photoionization process (Table 1), the experimental error being ±5%.[109] This has important consequences regarding the final damage, because radical cations and deprotonated radicals give rise to different reaction products.[111] For example, 8-oxo-7,8-dihydroguanine (8-oxodG; Figure 9b) and 2,6-diamino-4-hydroxy-5-formamidopyrimidine (FapydG) stem from radical cations, which undergo further reactions upon photon absorption.[112,113] Oxidative lesions resulting from deprotonated radicals include imidazolone, oxazolone, strand breaks and cross-links between purines and pyrimidines.[114,115]

Notwithstanding the important range of oxidative lesions reported in the literature, quantum yields are blatantly lacking. The reason is that, the large majority of studies were performed using external oxidants, which do not allow quantification of the final reaction products in respect to the initially generated radical cations. In addition, such experiments require that all the species added in the solutions (oxidants, buffer ingredients) are of high purity, because impurities may react with radicals formed at very low concentrations.[116]

A quantitative correlation of the final oxidative lesions with the initially formed radical cations can be achieved by combining time-resolved spectroscopy with analytical techniques. Although high-energy photoionization studies performed in the 1990s brought valuable information,[102,117,118] they encountered limitations in this respect, due to the fact that 193 nm laser pulses, ionize, not only the DNA, but also the water,[119] provoking side reactions. And the low-energy photoionization started to be systematically studied less than 10 years ago. The only quantum yield values associated with the latter studies concern 8-oxodG: it is 5×10^{-5} in calf thymus DNA irradiated at 254 and 295 nm,[82] corresponding to 2.5% of the UV generated radical cations, in perfect agreement with the finding that more than 95% of the radical cations undergo deprotonation.[36] A higher percentage (7%) was found for 8-oxodG formation in irradiated human telomeric G-quadruplexes, where part of the radical cations survive longer than in duplexes and have more time to react.[120] The fluorescence properties of 8-oxodG have been fully characterized; its emission spectrum peaks at 354 nm (Figure 7) and the Φ_{fl} is 5×10^{-5}.[86]

Despite the lack of quantitative characterization of the ensemble of lesions resulting from photoionization, recent publications provide interesting indications.

https://doi.org/10.1021/acsomega.4c02256
ACS Omega 2024, 9, 26826−26837

Kufner et al. developed a novel method for the detection of sequence-dependent UV damage with associated quantum yields.[121] After exposing a large number of short single strands to 266 nm irradiation, they observed damage in sequences GTGT and GGGT, in which photodimers are not expected to be formed. The latter could correspond to guanine-thymine cross-linked adducts resulting from deprotonated radicals.[115]

Carroll et al. reported that, after irradiation of polymeric $d(GC)_n \bullet d(GC)_n$ and $d(AT)_n \bullet d(AT)_n$ at 254 nm, they observed an important decrease (~30%) in the intensity of the initial absorption peak at ~260 nm; under the same irradiation conditions, the corresponding decrease observed for calf thymus DNA amounts to 53%.[21] These relative numbers cannot be explained by the induction of dimeric photoproducts, which are not expected to be formed in $d(GC)_n \bullet d(GC)_n$ and their yield in $d(AT)_n \bullet d(AT)_n$ should not exceed 3×10^{-5},[95] while it is 1.3×10^{-3} for calf thymus DNA.[79] In contrast, the Φ_i values of all three systems are quite similar: $1-2 \times 10^{-3}$ (Table 3).

The spectra obtained by Carroll et al. for $d(AT)_n \bullet d(AT)_n$ irradiated at 254 nm exhibit a red tail extended to, at least, 365 nm.[21] In contrast, the red tail induced by 254 nm irradiation of the dinucleotide dTpdA does not exceed 345 nm.[92] Using as irradiation source laser pulses at 266 nm and varying their intensity, it was established that the reaction products resulting from photoionization of $d(AT)_{10} \bullet d(AT)_{10}$ absorb at longer wavelengths compared to those due to photoreactions[99] (Figure 10). This is in agreement with the UV-induced absorption

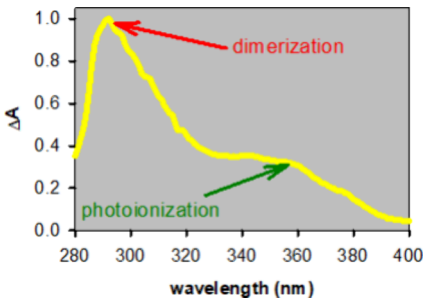

Figure 10. Difference between the steady-state absorption spectra recorded before and after irradiation of $d(AT)_{10} \bullet d(AT)_{10}$ with 266 nm laser pulses. Adapted from reference 99. Copyright RSC 2018.

spectra of dTpdA, which does not undergo one-photon ionization at 266 nm;[36] therefore, the red tail appearing upon their irradiation is limited to shorter wavelengths than that of $d(AT)_{10} \bullet d(AT)_{10}$ undergoing photoionization (Table 3).

5. EFFECTS OF THE DNA DAMAGE ON ITS FLUORESCENCE

According to the points discussed in the previous sections, the DNA damage will affect its intrinsic fluorescence in two ways. On the one hand, some of the generated lesions will emit at different wavelengths in respect to the undamaged DNA. On the other hand, lesion formation will alter the emission stemming from undamaged nucleobases. Below we compare the information conveyed by these two effects regarding the extent of DNA damage.

5.1. Lesion Fluorescence: Too Many Variables. The rational underlying the suggestion that lesion fluorescence can be used in order to check the efficacy of UV germicidal equipment is that this emission has well-identified features, which can be correlated with the degree of damage. But this is far from true. First, because the formation and the fluorescence quantum yields of 64PP, acting as internal fluorescent probes, strongly depend on the constitutive pyrimidines, the variations being higher than 1 order of magnitude (Table 2). Second, 64PP are probably not the most fluorescent lesions. In this respect, the findings by Carroll et al. are again very informative. The fluorescence spectra obtained following irradiation of calf thymus DNA at 254 nm peak at 402 nm. Surprisingly, the corresponding excitation spectra, as well as those recorded of $d(A)_n \bullet d(T)_n$, peak at 298 nm, i.e. they are blue-shifted by at least 17 nm compared to the absorption spectra of the three 64PP (Table 2). And, as these authors stressed, a similar fluorescence band, albeit less intense, appears upon irradiation of $d(AT)_n \bullet d(AT)_n$.

The above discrepancies are not surprising given that, despite the large number of final lesions that have been well characterized to date, many of them remain unknown. They concern in particular oxidative lesions ensuing from deprotonated radicals. Thus, the photoionization quantum yield at 266 nm (2×10^{-3}) of double-stranded calf thymus DNA[36] is roughly the same as the sum of the quantum yields determined for the ensemble of CPD and 64PP (1.4×10^{-3}) at 254 nm[79] (Table 1).

Another complication arises from the irradiation wavelength. As mentioned before, Φ_{CPD} is expected to remain roughly the same in the 200−300 nm range, while Φ_i increases by at least a factor of 10 when approaching 200 nm. This is due to modification of the photoionization mechanism and could be one reason for the better efficacy of far-UVC lamps to inactivate various types of microorganisms.[122] The same reasoning is valid for laser sources, capable of provoking two-photon ionization.[123] The corollary is that lesions with different emission properties are generated by each type of irradiation source. Some of them may emit, while others remain undetected upon monitoring fluorescence, the result being strongly dependent on the excitation wavelength. Thus, the fluorescence of calf thymus DNA induced by UV irradiation peaks at 402 nm when the excitation wavelength is 298 nm,[21] but excitation at 255 nm gives rise to a band peaking at 460 nm, exhibiting shoulders at ~400 and 420 nm (Figure 1). We note that in the former study irradiation was performed by means of a continuous light source emitting at 254 nm, while the latter using femtosecond laser pulses at 267 nm.[32]

5.2. Emission from Undamaged Nucleobases: A Promising Approach. As explained in Section 2, the fluorescence spectra of all B-form duplexes exhibit a peak at wavelengths shorter than 330 nm, even if, for some sequences, a second one, due to excimer/exciplex emission, is also present at longer wavelengths (Figures 1, 3 and 5). The "high -energy" peak is dominated by $\pi\pi^*$ transitions, localized or excitonic.

When a nucleobase disappears, its contribution to the fluorescence spectrum vanishes, independently of the type of the reaction taking place. But the fluorescence of undamaged neighboring nucleobases is also expected to be altered. As a matter of fact, the presence of lesions, and in particular those arising from reactions involving two nucleobases, such as photodimers or cross-links, induces structural distortions in their vicinity.[124−132] The nucleobases which were paired with those that have reacted lose their hydrogen bonding, become more flexible and the electronic coupling giving rise to exciton states is locally weakened.

The effect of the UV-induced DNA damage on the electronic coupling was examined by a study combining absorption

https://doi.org/10.1021/acsomega.4c02256
ACS Omega 2024, 9, 26826−26837

spectroscopy and mass spectrometry.[133] By comparing the behavior of $d(T)_{20}$ and $(A)_{20}\bullet d(T)_{20}$ irradiated at 266 nm, it was shown that the hypochromism, due to orbital overlap, decreases in the damaged region of the duplex with concomitant shift of the absorption maximum. This was attributed to the "local melting" of the complementary adenine strand. And, as explained in Section 2.3 (Figure 5), an increase in local flexibility provoked by CPD, which are not fluorescent, creates favorable conditions for the appearance of excimer/exciplex emission.

The combined result due to the vanishing of the reacting nucleobases and the enhanced flexibility of those located in their vicinity is the decrease in intensity of the high-energy peak, as observed in Figure 1. Furthermore, the low-energy emission is expected to increase because of excimer/exciplex fluorescence. But the latter band probably overlaps those stemming from various lesions and it is difficult to disentangle each contribution.

Finally, we note that, throughout this review, we focused specifically on the steady-state fluorescence spectra, because their modification is easier to be implemented in sensing applications. Yet, changes in the fluorescence lifetimes may be particularly informative regarding the DNA damage.

6. CONCLUSIONS AND PERSPECTIVES

From the above analysis, it appears that the fluorescence of the UV-induced reaction products cannot provide relevant information regarding the DNA damage. This is due to the multitude of final lesions, some of which have been fully characterized, but others remain, partially or completely, unknown. Given that the intensity and the position of the fluorescence band arising from the ensemble of the lesions depend on the quantum yields associated both with the formation and emission of each one of them, as well as of the individual absorption and fluorescence spectra, it is unlike to determine monitoring conditions that are valid for all types of irradiation sources (lasers, lamps) and irradiation wavelengths. In contrast, the $\pi\pi^*$ fluorescence stemming from undamaged nucleobases, located at wavelengths shorter than 330 nm and observed with excitation at the 255−270 nm range, is a promising perspective. A prerequisite for future developments is to examine in a systematic way the variation of this fluorescence as a function of the absorbed photons−the spectra in Figure 1 were simply obtained while searching for the optimal conditions to study the DNA fluorescence without damaging it.

The above conclusions were reached from fundamental studies performed on solutions with neutral pH, using purified nucleic acids and high purity salts for the buffer preparation, so that to grasp the intrinsic DNA properties. Molecular crowding in cells is expected to slow down the conformational motions and, consequently, enhance the DNA fluorescence (Section 2.3). But this effect has not been assessed so far. The cell fluorescence in the UV spectral domain is implicitly considered arising from other cellular components. Thus, two studies on bacteria associated arbitrarily an emission peak at 330 nm to a mixture of tyrosine and tryptophane while assigned to DNA a peak around 450 nm (for comparison see Figure 1). It is worthy to examine also this aspect in a systematic way, taking into account the current knowledge of the fundamental processes underlying the DNA fluorescence, especially because important viscosity changes in cells have been correlated with various diseases.[134]

In any case, the characterization of the intrinsic behavior of naked DNA in a quantitative way (in terms of quantum yields) constitutes a solid ground for apprehending more complex situations. Would this approach prove realistic, it could be possibly used for optoelectronic devices sensing of the damage caused, not only by UV irradiation, but also by other sanitizing agents and anticancer therapies.

AUTHOR INFORMATION

Corresponding Author

Dimitra Markovitsi − *Université Paris-Saclay, CNRS, Institut de Chimie Physique, UMR8000, 91405 Orsay, France;* orcid.org/0000-0002-2726-305X; Email: dimitra.markovitsi@universite-paris-saclay.fr

Complete contact information is available at: https://pubs.acs.org/10.1021/acsomega.4c02256

Notes

The author declares no competing financial interest.

ACKNOWLEDGMENTS

This work has received funding from the European Union's Horizon 2020 research and innovation programme under the Marie Sklodowska-Curie ITN programme (grant No. 765266 − LightDyNAmics).

REFERENCES

(1) Duan, X. R.; Liu, L. B.; Feng, F. D.; Wang, S. Cationic Conjugated Polymers for Optical Detection of DNA Methylation, Lesions, and Single Nucleotide Polymorphisms. *Acc. Chem. Res.* **2010**, *43*, 260−270.

(2) El-Yazbi, A. F.; Loppnow, G. R. Terbium fluorescence as a sensitive, inexpensive probe for UV-induced damage in nucleic acids. *Anal. Chim. Acta* **2013**, *786*, 116−123.

(3) El-Yazbi, A. F.; Loppnow, G. R. A selective, inexpensive probe for UV-induced damage in nucleic acids. *Can. J. Chem.* **2013**, *91*, 320−325.

(4) El-Yazbi, A. F.; Loppnow, G. R. Detecting UV-induced nucleic-acid damage. *TrAC, Trends Anal. Chem.* **2014**, *61*, 83−91.

(5) Condie, A. G.; Yan, Y.; Gerson, S. L.; Wang, Y. M. A Fluorescent Probe to Measure DNA Damage and Repair. *PLoS One* **2015**, *10*, e0131330.

(6) Li, R. Z.; Goswami, U.; Walck, M.; Khan, K.; Chen, J.; Cesario, T. C.; Rentzepis, P. M. Hand-held synchronous scan spectrometer for in situ and immediate detection of live/dead bacteria ratio. *Rev. Sci. Instrum.* **2017**, DOI: 10.1063/1.4991351.

(7) Li, R. Z.; Dhankhar, D.; Chen, J.; Cesario, T. C.; Rentzepis, P. M. Determination of live:dead bacteria as a function of antibiotic treatment. *J. Microbiol. Methods* **2018**, *154*, 73−78.

(8) El-Yazbi, A. F.; Loppnow, G. R. Probing DNA damage induced by common antiviral agents using multiple analytical techniques. *Pharm. Biomed. Anal.* **2018**, *157*, 226−234.

(9) Li, R. Z.; Goswami, U.; King, M.; Chen, J.; Cesario, T. C.; Rentzepis, P. M. In situ detection of live-to-dead bacteria ratio after inactivation by means of synchronous fluorescence and PCA. *Proc. Natl. Acad.Sci. U.S.A.* **2018**, *115*, 668−673.

(10) Peng, Q.; Weng, K. G.; Li, S. T.; Xu, R.; Wang, Y. X.; Wu, Y. Z. A Perspective of Epigenetic Regulation in Radiotherapy. *Front. Cell Dev. Biol.* **2021**, *9*, 624312.

(11) Fadhil, E. A. A.; Abdullah, M. M.; Lafta, F. M. Preparation of N-A Cysteine-capped CdTe/CdS/ZnS core/shell/shell QDs as a Selective Probe for Detecting Damaged DNA. *Inter. J. Nanosci.* **2024**, DOI: 10.1142/S0219581X23500618.

(12) Hauswirth, W.; Wang, S.Y. Pyrimidine adduct fluorescence in UV irradiated nucleic acids. *Biochem. Biophys. Res. Commun.* **1973**, *51*, 819−826.

(13) Hadi, J.; Dunowska, M.; Wu, S. Y.; Brightwell, G. Control Measures for SARS-CoV-2: A Review on Light-Based Inactivation of Single-Stranded RNA Viruses. *Pathogens* **2020**, *9*, 737.

(14) Luo, H.; Zhong, L. X. Ultraviolet germicidal irradiation (UVGI) for in-duct airborne bioaerosol disinfection: Review and analysis of design factors. *Build. Environ.* **2021**, *197*, 107852.
(15) Trivellin, N.; Piva, F.; Fiorimonte, D.; Buffolo, M.; De Santi, C.; Orlandi, V. T.; Dughiero, F.; Meneghesso, G.; Zanoni, E.; Meneghini, M. UV-Based Technologies for SARS-CoV2 Inactivation: Status and Perspectives. *Electronics* **2021**, *10*, 1703.
(16) Ambardar, S.; Howell, M. C.; Mayilsamy, K.; McGill, A.; Green, R.; Mohapatra, S.; Voronine, D. V.; Mohapatra, S. S. Ultrafast-UV laser integrating cavity device for inactivation of SARS-CoV-2 and other viruses. *Sci. Rep.* **2022**, DOI: 10.1038/s41598-022-13670-8.
(17) Michelini, Z.; Mazzei, C.; Magurano, F.; Baggieri, M.; Marchi, A.; Andreotti, M.; Cara, A.; Gaudino, A.; Mazzalupi, M.; Antonelli, F.; Sommella, L.; Angeletti, S.; Razzano, E.; Runge, A.; Petrinca, P. UltraViolet SANitizing System for Sterilization of Ambulances Fleets and for Real-Time Monitoring of Their Sterilization Level. *Int. J. Environ. Res. Public Health* **2022**, *19*, 331.
(18) Sun, K. X.; Niu, G.; Zhang, Y. F.; Yang, J.; Zhang, D. N.; Wu, H.; Shao, X. Y.; Ma, X. Q. Ultrafast inactivation of SARS-CoV-2 with 266 nm lasers. *Sci. Rep.* **2022**, DOI: 10.1038/s41598-022-23423-2.
(19) Barber, V. P.; Goss, M. B.; Franco Deloya, L. J.; LeMar, L. N.; Li, Y.; Helstrom, E.; Canagaratna, M.; Keutsch, F. N.; Kroll, J. H. Indoor Air Quality Implications of Germicidal 222 nm Light. *Environ. Sci. Technol.* **2023**, *57*, 15990−15998.
(20) Nagpal, A.; Dhankhar, D.; Cesario, T. C.; Li, R. Z.; Chen, J.; Rentzepis, P. M. Thymine dissociation and dimer formation: A Raman and synchronous fluorescence spectroscopic study. *Proc. Natl. Acad.Sci. U.S.A.* **2021**, DOI: 10.1073/pnas.2025263118.
(21) Carroll, G. T.; Dowling, R. C.; Kirschman, D. L.; Masthay, M. B.; Mammana, A. Intrinsic fluorescence of UV-irradiated DNA. *J. Photochem. Photobiol. A: Chem.* **2023**, *437*, 114484.
(22) Markovitsi, D.; Onidas, D.; Talbot, F.; Marguet, S.; Gustavsson, T.; Lazzarotto, E. UVB/UVC induced processes in model DNA helices studied by time-resolved spectroscopy: pitfalls and tricks. *J. Photochem. Photobiol. A-Chem.* **2006**, *183*, 1−8.
(23) Gustavsson, T.; Markovitsi, D. Fundamentals of the Intrinsic DNA Fluorescence. *Acc. Chem. Res.* **2021**, *54*, 1226−1235.
(24) Kwok, W. M.; Ma, C. S.; Phillips, D. L. "Bright" and "Dark" excited states of an alternating AT oligomer characterized by femtosecond broadband spectroscopy. *J. Phys. Chem. B* **2009**, *113*, 11527−11534.
(25) Schwalb, N. K.; Temps, F. Base sequence and higher-order structure induce the complex excited-state dynamics in DNA. *Science* **2008**, *322*, 243−245.
(26) Peon, J.; Zewail, A. H. DNA/RNA nucleotides and nucleosides: direct measurement of excited-state lifetimes by femtosecond fluorescence up-conversion. *Chem. Phys. Lett.* **2001**, *348*, 255−262.
(27) Martinez-Fernandez, L.; Santoro, F.; Improta, R. Nucleic Acids as a Playground for the Computational Study of the Photophysics and Photochemistry of Multichromophore Assemblies. *Acc. Chem. Res.* **2022**, *55*, 2077−2087.
(28) Zuffo, M.; Gandolfini, A.; Heddi, B.; Granzhan, A. Harnessing intrinsic fluorescence for typing of secondary structures of DNA. *Nucl. Ac. Res.* **2020**, *48*, No. e61.
(29) Xiang, X.; Li, Y.; Ling, L.; Bao, Y.; Su, Y.; Guo, X. Label-free and dye-free detection of target DNA based on intrinsic fluorescence of the (3 + 1) interlocked bimolecular G-quadruplexes. *Sens. Actuators B Chem.* **2019**, *290*, 68−72.
(30) Lopez, A.; Liu, J. Probing metal-dependent G-quadruplexes using the intrinsic fluorescence of DNA. *Chem. Commun.* **2022**, *58*, 10225−10228.
(31) Assi, S.; Abbas, I.; Arafat, B.; Evans, K.; Al-Jumeily, D. Authentication of Covid-19 Vaccines Using Synchronous Fluorescence Spectroscopy. *J. Fluoresc.* **2023**, *33*, 1165−1174.
(32) Vayá, I.; Gustavsson, T.; Miannay, F. A.; Douki, T.; Markovitsi, D. Fluorescence of natural DNA: from the femtosecond to the nanosecond time-scales. *J. Am. Chem. Soc.* **2010**, *132*, 11834−11835.
(33) Wagenknecht, H. A. Remote Photodamaging of DNA by Photoinduced Energy Transport. *Chembiochem* **2022**, *23*, No. e202100265.
(34) Kufner, C. L.; Crucilla, S.; Ding, D.; Stadlbauer, P.; Sponer, J.; Szostak, J. W.; Sasselov, D. D.; Szabla, R. Photoinduced charge separation and DNA self-repair depend on sequence directionality and stacking pattern. *Chem. Sci.* **2024**, *15*, 2158−2166.
(35) Schroeder, C. A.; Pluharova, E.; Seidel, R.; Schroeder, W. P.; Faubel, M.; Slavicek, P.; Winter, B.; Jungwirth, P.; Bradforth, S. E. Oxidation Half-Reaction of Aqueous Nucleosides and Nucleotides via Photoelectron Spectroscopy Augmented by ab Initio Calculations. *J. Am. Chem. Soc.* **2015**, *137*, 201−209.
(36) Balanikas, E.; Banyasz, A.; Douki, T.; Baldacchino, G.; Markovitsi, D. Guanine Radicals Induced in DNA by Low-Energy Photoionization. *Acc. Chem. Res.* **2020**, *53*, 1511−1519.
(37) Kwok, W.-M.; Ma, C.; Phillips, D. L. Femtosecond time- and wavelength-resolved fluorescence and absorption study of the excited states of adenosine and an adenine oligomer. *J. Am. Chem. Soc.* **2006**, *128*, 11894−11905.
(38) Kwok, W. M.; Ma, C.; Phillips, D. L. A doorway state leads to photostability or triplet photodamage in thymine DNA. *J. Am. Chem. Soc.* **2008**, *130*, 5131−5139.
(39) Ma, C. S.; Chan, R. C.-T.; Chan, C. T.-L.; Wong, A. K.-W.; Kwok, W.-M. Real-time Monitoring Excitation Dynamics of Human Telomeric Guanine Quadruplexes: Effect of Folding Topology, Metal Cation, and Confinement by Nanocavity Water Pool. *J. Phys. Chem. Lett.* **2019**, *10*, 7577−7585.
(40) Schwalb, N.; Temps, F. Ultrafast electronic excitation in guanosine is promoted by hydrogen bonding with cytidine. *J. Am. Chem. Soc.* **2007**, *129*, 9272−9273.
(41) Stuhldreier, M. C.; Temps, F. Ultrafast photo-initiated molecular quantum dynamics in the DNA dinucleotide d(ApG) revealed by broadband transient absorption spectroscopy. *Faraday Disc.* **2013**, *163*, 173−188.
(42) Gustavsson, T.; Markovitsi, D. The Ubiquity of High-Energy Nanosecond Fluorescence in DNA Duplexes. *J. Phys. Chem. Lett.* **2023**, *14*, 2141−2147.
(43) Markovitsi, D. Processes triggered in guanine quadruplexes by direct absorption of UV radiation: From fundamental studies toward optoelectronic biosensors. *Photochem. Photobiol.* **2024**, *100*, 262−274.
(44) Ballini, J. P.; Vigny, P.; Daniels, M. Synchrotron excitation of DNA fluorescence: decay time evidence for excimer emission at room temperature. *Biophys. Chem.* **1983**, *18*, 61−65.
(45) Onidas, D.; Markovitsi, D.; Marguet, S.; Sharonov, A.; Gustavsson, T. Fluorescence properties of DNA nucleosides and nucleotides: a refined steady-state and femtosecond investigation. *J. Phys. Chem. B* **2002**, *106*, 11367−11374.
(46) Improta, R.; Santoro, F.; Blancafort, L. Quantum Mechanical Studies on the Photophysics and the Photochemistry of Nucleic Acids and Nucleobases. *Chem. Rev.* **2016**, *116*, 3540−3593.
(47) Sharonov, A.; Gustavsson, T.; Marguet, S.; Markovitsi, D. Photophysical properties of 5-methylcytidine. *Photochem. & Photobiol. Sci.* **2003**, *2*, 362−364.
(48) Wang, D. H.; Wang, X. L.; Jiang, Y. R.; Cao, S. M.; Jin, P. P.; Pan, H. F.; Sun, H. T.; Sun, Z. R.; Chen, J. Q. Excited State Dynamics of Methylated Guanosine Derivatives Revealed by Femtosecond Time-resolved Spectroscopy. *Photochem. Photobiol.* **2022**, *98*, 1008−1016.
(49) Banyasz, A.; Douki, T.; Improta, R.; Gustavsson, T.; Onidas, D.; Vayá, I.; Perron, M.; Markovitsi, D. Electronic Excited States Responsible for Dimer Formation upon UV Absorption Directly by Thymine Strands: Joint Experimental and Theoretical Study. *J. Am. Chem. Soc.* **2012**, *134*, 14834−14845.
(50) Banyasz, A.; Gustavsson, T.; Onidas, D.; Changenet-Barret, P.; Markovitsi, D.; Improta, R. Multi-Pathway Excited State Relaxation of Adenine Oligomers in Aqueous Solution: A Joint Theoretical and Experimental Study. *Chem. Eur. J.* **2013**, *19*, 3762−3774.
(51) Vayá, I.; Brazard, J.; Gustavsson, T.; Markovitsi, D. Electronically excited states of DNA oligonucleotides with disordered base sequences

https://doi.org/10.1021/acsomega.4c02256
ACS Omega 2024, 9, 26826−26837

studied by fluorescence spectroscopy'. *Photochem. & Photobiol. Sci.* **2012**, *11*, 1767−1773.
(52) Sutherland, J. C.; Griffin, K. P. Absorption spectrum of DNA for wavelengths greater than 300 nm. *Radiat. Res.* **1981**, *86*, 399−410.
(53) Mouret, S.; Philippe, C.; Gracia-Chantegrel, J.; Banyasz, A.; Karpati, S.; Markovitsi, D.; Douki, T. UVA-induced cyclobutane pyrimidine dimers in DNA: a direct photochemical mechanism? *Org. Biomol. Chem.* **2010**, *8*, 1706−1711.
(54) Banyasz, A.; Vayá, I.; Changenet-Barret, P.; Gustavsson, T.; Douki, T.; Markovitsi, D. Base-pairing enhances fluorescence and favors cyclobutane dimer formation induced upon absorption of UVA radiation by DNA. *J. Am. Chem. Soc.* **2011**, *133*, 5163−5165.
(55) Plasser, F.; Aquino, A.; Lischka, H.; Nachtigallová, D. Electronic Excitation Processes in Single-Strand and Double-Strand DNA: A Computational Approach. *Top. Curr. Chem.* **2014**, *356*, 1−38.
(56) Varsano, D.; Di Felice, R.; Marques, M. A. L.; Rubio, A. A TDDFT study of the excited states of DNA bases and their assemblies. *J. Phys. Chem. B* **2006**, *110*, 7129−7138.
(57) Spata, V. A.; Matsika, S. Role of Excitonic Coupling and Charge-Transfer States in the Absorption and CD Spectra of Adenine-Based Oligonucleotides Investigated through QM/MM Simulations. *J. Phys. Chem. A* **2014**, *118*, 12021−12030.
(58) Bouvier, B.; Dognon, J. P.; Lavery, R.; Markovitsi, D.; Millié, P.; Onidas, D.; Zakrzewska, K. Influence of conformational dynamics on the exciton states of DNA oligomers. *J. Phys. Chem. B* **2003**, *107*, 13512−13522.
(59) Nogueira, J. J.; Plasser, F.; Gonzalez, L. Electronic delocalization, charge transfer and hypochromism in the UV absorption spectrum of polyadenine unravelled by multiscale computations and quantitative wavefunction analysis. *Chem. Sci.* **2017**, *8*, 5682−5691.
(60) Zuo, X.; Cui, G.; Merz, K. M., Jr; Zhang, L.; Lewis, F. D.; Tiede, D. M. X-ray diffraction "fingerprinting" of DNA structure in solution for quantitative evaluation of molecular dynamics simulation. *Proc. Natl. Acad. Sci. U.S.A.* **2006**, *103*, 3534−3539.
(61) Hithell, G.; Donaldson, P. M.; Greetham, G. M.; Towrie, M.; Parker, A. W.; Burley, G. A.; Hunt, N. T. Effect of oligomer length on vibrational coupling and energy relaxation in double-stranded DNA. *Chem. Phys.* **2018**, *512*, 154−164.
(62) Guilbaud, S.; Salome, L.; Destainville, N.; Manghi, M.; Tardin, C. Dependence of DNA Persistence Length on Ionic Strength and Ion Type. *Phys. Rev. Lett.* **2019**, *122*, 028102.
(63) Markovitsi, D.; Gustavsson, T.; Vayá, I. Fluorescence of DNA Duplexes: From Model Helices to Natural DNA. *J. Phys. Chem. Lett.* **2010**, *1*, 3271−3276.
(64) Huix-Rotllant, M.; Brazard, J.; Improta, R.; Burghardt, I.; Markovitsi, D. Stabilization of mixed Frenkel-charge transfer excitons extended across both strands of guanine-cytosine DNA duplexes. *J. Phys. Chem. Lett.* **2015**, *6*, 2247−2251.
(65) Ge, G.; Georghiou, S. Excited-state properties of the alternating polynucleotide poly(dA-dT)poly(dA-dT). *Photochem. Photobiol.* **1991**, *54*, 301−305.
(66) Vayá, I.; Brazard, J.; Huix-Rotllant, M.; Thazhathveetil, A.; Lewis, F.; Gustavsson, T.; Burghardt, I.; Improta, R.; Markovitsi, D. High energy long-lived mixed Frenkel - charge transfer excitons: from double-stranded $(AT)_n$ to natural DNA. *Chem. Eur. J.* **2016**, *22*, 4904−4914.
(67) Vaya, I.; Gustavsson, T.; Markovitsi, D. High-Energy Long-Lived Emitting Mixed Excitons in Homopolymeric Adenine-Thymine DNA Duplexes. *Molecules* **2022**, *27*, 3558.
(68) Improta, R.; Barone, V. Interplay between "neutral" and "charge-transfer" excimers rules the excited state decay in adenine-rich polynucleotides. *Angew. Chem., Int. Ed.* **2011**, *50*, 12016−12019.
(69) Georghiou, S.; Kubala, S. M.; Large, C. C. Environmental control of deformability of the DNA double helix. *Photochem. Photobiol.* **1998**, *67*, 526−531.
(70) Eisinger, J.; Shulman, R. G. Precursor of thymine dimer in ice. *Proc. Natl. Acad. Sci. U.S.A.* **1967**, *58*, 895.
(71) Eisinger, J.; Gueron, M.; Shulman, R. G.; Yamane, T. Excimer fluorescence of dinucleotides and polynuceotides. *Proc. Natl. Acad. Sci. U.S.A.* **1966**, *55*, 1015.
(72) Shih, C. C.; Georghiou, S. Large-amplitude fast motions in double-stranded DNA driven by solvent thermal fluctuations. *Biopolymers* **2006**, *81*, 450−463.
(73) Cadet, J.; Grand, A.; Douki, T. Solar UV radiation-induced DNA Bipyrimidine photoproducts: formation and mechanistic insights. *Top. Curr. Chem.* **2014**, *356*, 249−75.
(74) Lemaire, D.; Ruzsicska, B. P. Quantum yields and secondary photoreactions of the photoproducts of dTpdT, dTpdC and dTpdU. *Photochem. Photobiol.* **1993**, *57*, 755−769.
(75) McCullagh, M.; Hariharan, M.; Lewis, F. D.; Markovitsi, D.; Douki, T.; Schatz, G. C. Conformational control of TT dimerization in DNA conjugates. A molecular dynamics study. *J. Phys. Chem. B* **2010**, *114*, 5215−5221.
(76) Lee, W.; Matsika, S. Role of charge transfer states into the formation of cyclobutane pyrimidine dimers in DNA. *Faraday Disc.* **2019**, *216*, 507−519.
(77) Schreier, W. J.; Schrader, T. B.; Koller, F. O.; Gilch, P.; Crespo-Hernàndez, C.; Swaminathan, V. N.; Carell, T.; Zinth, W.; Kohler, B. Thymine dimerization in DNA is an ultrafast photoreaction. *Science* **2007**, *315*, 625−629.
(78) Markovitsi, D. UV-induced DNA Damage: The Role of Electronic Excited States. *Photochem. Photobiol.* **2016**, *92*, 45−51.
(79) Douki, T. Effect of denaturation on the photochemistry of pyrimidine bases in isolated DNA. *J. Photochem. Photobiol. B* **2006**, *82*, 45−52.
(80) Clingen, P. H.; Davies, R. J. H. Quantum yields of adenine photodimerization in poly(deoxyadenylic acid) and DNA. *J. Photochem. Photobiol. B-Biol.* **1997**, *38*, 81−87.
(81) Bose, S. N.; Davies, R. J. H. The photoreactivity of T-A Ssequences in oligodeoxyribonucleotides and DNA. *Nucl. Ac. Res.* **1984**, *12*, 7903−7914.
(82) Gomez-Mendoza, M.; Banyasz, A.; Douki, T.; Markovitsi, D.; Ravanat, J. L. Direct Oxidative Damage of Naked DNA Generated upon Absorption of UV Radiation by Nucleobases. *J. Phys. Chem. Lett.* **2016**, *7*, 3945−3948.
(83) Marguet, S.; Markovitsi, D. Time-resolved study of thymine dimer formation. *J. Am. Chem. Soc.* **2005**, *127*, 5780−5781.
(84) Blais, J.; Douki, T.; Vigny, P.; Cadet, J. Fluorescence quantum yield determination of pyrymidine (6−4) pyrimidone photoadducts. *Photochem. Photobiol.* **1994**, *59*, 402−404.
(85) Douki, T.; Voituriez, L.; Cadet, J. Measurement of pyrimidine (6−4) photoproducts in DNA by a mild acidic hydrolysis-HPLC fluorescence detection assay. *Chem. Res. Toxicol.* **1995**, *8*, 244−253.
(86) Changenet-Barret, P.; Gustavsson, T.; Improta, R.; Markovitsi, D. Ultrafast Excited-State Deactivation of 8-Hydroxy-2′-deoxyguanosine Studied by Femtosecond Fluorescence Spectroscopy and Quantum-Chemical Calculations. *J. Phys. Chem. A* **2015**, *119*, 6131−6139.
(87) Douki, T.; Sage, E. Dewar valence isomers, the third type of environmentally relevant DNA photoproducts induced by solar radiation. *Photochem. & Photobiol. Sci.* **2016**, *15*, 24−30.
(88) Fingerhut, B. P.; Herzog, T. T.; Ryseck, G.; Haiser, K.; Graupner, F. F.; Heil, K.; Gilch, P.; Schreier, W. J.; Carell, T.; de Vivie-Riedle, R.; Zinth, W. Dynamics of ultraviolet-induced DNA lesions: Dewar formation guided by pre-tension induced by the backbone. *New J. Phys.* **2012**, *14*, 065006.
(89) Setlow, P.; Li, L. Photochemistry and Photobiology of the Spore Photoproduct: A 50-Year Journey. *Photochem. Photobiol.* **2015**, *91*, 1263−1290.
(90) Kumar, S.; Joshi, P. C.; Sharma, N. D.; Bose, S. N.; Davies, R. J. H.; Takeda, N.; McCloskey, J. A. Adenine Photodimerization in Deoxyadenylate Sequences - Elucidation of the Mechanism through Structural Studies of a Major d(ApA) Photoproduct. *Nucl. Ac. Res.* **1991**, *19*, 2841−2847.
(91) Banyasz, A.; Martinez-Fernandez, L.; Ketola, T.; Muñoz-Losa, A.; Esposito, L.; Markovitsi, D.; Improta, R. Excited State Pathways

https://doi.org/10.1021/acsomega.4c02256
ACS Omega 2024, 9, 26826−26837

Leading to Formation of Adenine Dimers. *J. Phys. Chem. Lett.* **2016**, *7*, 2020−2023.
(92) Bose, S. N.; Kumar, S.; Davies, R. J. H.; Sethi, S. K.; McCloskey, J. A. The Photochemistry of d(T-A) in Aqueous Solution and Ice. *Nucl. Ac. Res.* **1984**, *12*, 7929−7947.
(93) Davies, R. J. H.; Malone, J. F.; Gan, Y.; Cardin, C. J.; Lee, M. P. H.; Neidle, S. High-resolution crystal structure of the intramolecular d(TpA) thymine-adenine photoadduct and its mechanistic implications. *Nucl. Ac. Res.* **2007**, *35*, 1048−1053.
(94) Martinez-Fernandez, L.; Improta, R. Novel adenine/thymine photodimerization channels mapped by PCM/TD-DFT calculations on dApT and TpdA dinucleotides. *Photochem. & Photobiol. Sci.* **2017**, *16*, 1277−1283.
(95) Asgatay, S.; Martinez, A.; Coantic-Castex, S.; Harakat, D.; Philippe, C.; Douki, T.; Clivio, P. UV-Induced TA Photoproducts: Formation and Hydrolysis in Double-Stranded DNA. *J. Am. Chem. Soc.* **2010**, *132*, 10260−10261.
(96) Gasparro, F. P.; Fresco, J. R. Ultraviolet-induced 8,8-adenine dehydromers in oligonucleotides and polynucleotides. *Nucl. Ac. Res.* **1986**, *14*, 4239−4251.
(97) Douki, T.; Angelov, D.; Cadet, J. UV laser photolysis of DNA: effect of duplex stability on charge-transfer efficiency. *J. Am. Chem. Soc.* **2001**, *123*, 11360−11366.
(98) Cadet, J.; Wagner, J. R.; Angelov, D. Biphotonic Ionization of DNA: From Model Studies to Cell. *Photochem. Photobiol.* **2019**, *95*, 59−72.
(99) Banyasz, A.; Ketola, T.; Martinez-Fernandez, L.; Improta, R.; Markovitsi, D. Adenine radicals generated in alternating AT duplexes by direct absorption of low-energy UV radiation. *Faraday Disc.* **2018**, *207*, 181−197.
(100) Kawai, K.; Fujitsuka, M.; Majima, T. Selective guanine oxidation by UVB-irradiation in telomeric DNA. *Chem. Commun.* **2005**, 1476−1477.
(101) Balanikas, E.; Markovitsi, D. DNA photoionization: from high to low energies. In *DNA Photodamage: From Light Absorption to Cellular Responses and Skin Cancer*; Improta, R., Douki, T., Eds.; RSC: Cambridge, 2021; pp 37−54.
(102) Candeias, L. P.; O'Neill, P.; Jones, G. D. D.; Steenken, S. Ionization of polynucleotides and DNA in aqueous solution by 193 nm pulsed laser light - identification of base-derived radicals. *Int. J. Radiat. Biol.* **1992**, *61*, 15−20.
(103) Melvin, T.; Plumb, M. A.; Botchway, S. W.; O'Neill, P.; Parker, A. W. 193 nm Light Induces Single-strand Breakage of DNA Predominantly at Guanine. *Photochem. Photobiol.* **1995**, *61*, 584−591.
(104) Bucher, D. B.; Pilles, B. M.; Carell, T.; Zinth, W. Charge separation and charge delocalization identified in long-living states of photoexcited DNA. *Proc. Natl. Acad. Sci. U.S.A.* **2014**, *111*, 4369−4374.
(105) Candeias, L. P.; Steenken, S. Electron transfer in di(deoxy)-nucleoside phosphates in aqueous solution: rapid migration of oxidative damage (via adenine) to guanine. *J. Am. Chem. Soc.* **1993**, *115*, 2437−2440.
(106) Melvin, T.; Botchway, S.; Parker, A. W.; O'Neill, P. Migration of photoinuced oxidative damage in models for DNA. *Chem. Commun.* **1995**, 653−654.
(107) Matsunaga, T.; Hieda, K.; Nikaido, O. Wavelength Dependent Formation of Thymine Dimers and (6−4)Photoproducts in DNA by Monochromatic Ultraviolet Light Ranging from 150 to 365 nm. *Photochem. Photobiol.* **1991**, *54*, 403−410.
(108) Balanikas, E. *Low-energy photoionization of guanine quadruplexes*; PhD Thesis, Paris Saclay University, 2021.
(109) Balanikas, E.; Banyasz, A.; Baldacchino, G.; Markovitsi, D. Deprotonation Dynamics of Guanine Radical Cations. *Photochem. Photobiol.* **2022**, *98*, 523−531.
(110) Kobayashi, K.; Tagawa, S. Direct observation of guanine radical cation deprotonation in duplex DNA using pulse radiolysis. *J. Am. Chem. Soc.* **2003**, *125*, 10213−10218.
(111) Cadet, J.; Douki, T.; Ravanat, J. L. Oxidatively generated damage to the guanine moiety of DNA: Mechanistic aspects and formation in cells. *Acc. Chem. Res.* **2008**, *41*, 1075−1083.
(112) Shukla, L. I.; Pazdro, R.; Huang, J.; DeVreugd, C.; Becker, D.; Sevilla, M. D. The formation of DNA sugar radicals from photo-excitation of guanine cation radicals. *Radiat. Res.* **2004**, *161*, 582−590.
(113) Adhikary, A.; Malkhasian, A. Y. S.; Collins, S.; Koppen, J.; Becker, D.; Sevilla, M. D. UVA-visible photo-excitation of guanine radical cations produces sugar radicals in DNA and model structures. *Nucl. Ac. Res.* **2005**, *33*, 5553−5564.
(114) Cadet, J.; Wagner, J. R.; Shafirovich, V.; Geacintov, N. E. One-electron oxidation reactions of purine and pyrimidine bases in cellular DNA. *Int. J. Radiat. Biol.* **2014**, *90*, 423−432.
(115) Labet, V.; Morell, C.; Grand, A.; Cadet, J.; Cimino, P.; Barone, V. Formation of cross-linked adducts between guanine and thymine mediated by hydroxyl radical and one-electron oxidation: a theoretical study. *Organic & Biomolecular Chemistry* **2008**, *6*, 3300−3305.
(116) Balanikas, E.; Banyasz, A.; Baldacchino, G.; Markovitsi, D. Populations and Dynamics of Guanine Radicals in DNA strands: Direct versus Indirect Generation. *Molecules* **2019**, *24*, 2347.
(117) Candeias, L. P.; Steenken, S. Ionization of purine nucleosides and nucleotides and their components by 193-nm laser photolysis in aqueous solution: model studies for oxidative damage of DNA. *J. Am. Chem. Soc.* **1992**, *114*, 699−704.
(118) Melvin, T.; Botchway, S. W.; Parker, A. W.; O'Neill, P. Induction of strand breaks in single-stranded polyribonucleotides and DNA by photoionization: One electron oxidized nucleobase radicals as precursors. *J. Am. Chem. Soc.* **1996**, *118*, 10031−10036.
(119) Bartels, D. M.; Crowell, R. A. Photoionization yield vs energy in H_2O and D_2O. *J. Phys. Chem. A* **2000**, *104*, 3349−3355.
(120) Banyasz, A.; Martinez-Fernandez, L.; Balty, C.; Perron, M.; Douki, T.; Improta, R.; Markovitsi, D. Absorption of Low-Energy UV Radiation by Human Telomere G-Quadruplexes Generates Long-Lived Guanine Radical Cations. *J. Am. Chem. Soc.* **2017**, *139*, 10561−10568.
(121) Kufner, C. L.; Crucilla, S.; Ding, D.; Stadlbauer, P.; Sponer, J.; Szostak, J. W.; Sasselov, D. D.; Szabla, R. Photoinduced charge separation and DNA self-repair depend on sequence directionality and stacking pattern. *Chem. Sci.* **2024**, *15*, 2158.
(122) Ma, B.; Gundy, P. M.; Gerba, C. P.; Sobsey, M. D.; Linden, K. G. UV Inactivation of SARS-CoV-2 across the UVC Spectrum: KrCl* Excimer, Mercury-Vapor, and Light-Emitting-Diode (LED) Sources. *Appl. Environ. Microbiol.* **2021**, DOI: 10.1128/AEM.01532-21.
(123) Morkunas, V.; Urbonaite, G.; Gabryte-Butkiene, E.; Sobutas, S.; Vengris, M.; Danielius, R.; Ruksenas, O. DNA-Damaging Effect of Different Wavelength (206 and 257 nm) Femtosecond Laser Pulses. *Photobiomodul. Photomed. Laser Sur.* **2019**, *37*, 254−261.
(124) Wang, C.-I.; Taylor, J. S. Site specific effect of thymine dimer formation on $dA_n.dT_n$ track bending and its biological implications. *Proc. Natl. Acad. Sci. U.S.A.* **1991**, *88*, 9072−9076.
(125) Kim, J. K.; Patel, D.; Choi, B. S. Contrasting structural impacts induced by cis-syn cyclobutane dimer and (6−4)-adduct in DNA duplex decamers - implication in mutagenesis and repair reactivity. *Photochem. Photobiol.* **1995**, *62*, 44−50.
(126) Miaskiewicz, K.; Miller, J.; Cooney, M.; Osman, R. Computational simulations of DNA distortions by a cis,syn-cyclobutane thymine dimer lesion. *J. Am. Chem. Soc.* **1996**, *118*, 9156−9163.
(127) Spector, T. I.; Cheatham, T. E.; Kollman, P. A. Unrestrained molecular dynamics of photodamaged DNA in aqueous solution. *J. Am. Chem. Soc.* **1997**, *119*, 7095−7104.
(128) McAteer, K.; Jing, Y.; Kao, J.; Taylor, J. S.; Kennedy, M. A. Solution-state structure of a DNA dodecamer duplex containing a *cis-syn* thymine cyclobutane dimer, the major UV photoproduct of DNA. *J. Mol. Biol.* **1998**, *282*, 1013−1032.
(129) Lukin, M.; de los Santos, C. NMR structures of damaged DNA. *Chem. Rev.* **2006**, *106*, 607−686.
(130) Park, C. J.; Lee, J. H.; Choi, B. S. Functional insights gained from structural analyses of DNA duplexes that contain UV-damaged photoproducts. *Photochem. Photobiol.* **2007**, *83*, 187−195.
(131) O'Neil, L. L.; Wiest, O. Structures and energetics of base flipping of the thymine dimer depend on DNA sequence. *J. Phys. Chem. B* **2008**, *112*, 4113−4122.

https://doi.org/10.1021/acsomega.4c02256
ACS Omega 2024, 9, 26826−26837

(132) Knips, A.; Zacharias, M. Influence of a cis,syn-Cyclobutane Pyrimidine Dimer Damage on DNA Conformation Studied by Molecular Dynamics Simulations. *Biopolymers* **2015**, *103*, 215−226.
(133) Banyasz, A.; Karpati, S.; Lazzarotto, E.; Markovitsi, D.; Douki, T. UV-Induced structural changes of model DNA helices probed by optical spectroscopy. *J. Phys. Chem. C* **2009**, *113*, 11747−11750.
(134) Clancy, E.; Ramadurai, S.; Needham, S. R.; Baker, K.; Eastwood, T. A.; Weinstein, J. A.; Mulvihill, D. P.; Botchway, S. W. Fluorescence and phosphorescence lifetime imaging reveals a significant cell nuclear viscosity and refractive index changes upon DNA damage. *Sci. Rep.* **2023**, DOI: 10.1038/s41598-022-26880-x.

https://doi.org/10.1021/acsomega.4c02256
ACS Omega 2024, 9, 26826−26837